ACS Pharmacology & Translational Science

pubs.acs.org/ptsci Article

Development of a Cell-Based Recombinant Green Fluorescent Protein Assay System for Generalized Discovery of Viral Protease Inhibitors

Yan Feng,[†] Xiaoyan Wu,[†] Ruiting Chen,[†] Yao Fan, Changping Xu, Chenjie Fang, Huimin Sun, Shuling Jian, Jiasheng Song,[‡] and Beibei Wu*[,‡]

Cite This: ACS Pharmacol. Transl. Sci. 2025, 8, 3944−3952 Read Online

ACCESS | Metrics & More | Article Recommendations | Supporting Information

ABSTRACT: Viral proteases are critical targets for antiviral drug development, but current screening methods for protease inhibitors often require high biosafety levels or lack cell-based relevance. Here, we developed a novel cell-based assay system utilizing recombinant green fluorescent protein (GFP) technology, designated as DIFF-recombinant GFP (DIFF-rGFP), for potentially high-throughput screening of viral protease inhibitors. By systematically investigating potential insertion sites within the green fluorescent protein (GFP), we constructed a series of recombinant green fluorescent proteins (rGFPs) that accommodate exogenous protease cleavage sequences. Using the 3-Chymotrypsin like protease ($3CL^{pro}$) of severe acute respiratory syndrome coronavirus-2 (SARS-CoV-2) as a model, we demonstrated that the DIFF-rGFP assay relies on the coexpression of rGFP and the protease, with fluorescence intensity increasing upon inhibitor action. This assay eliminates the need for high biosafety laboratories and is performed at the cellular level. For proof of concept, we validated this method using two well-characterized SARS-CoV-2 $3CL^{pro}$ inhibitors, GC376 and ensitrelvir, to demonstrate its applicability for inhibitor screening. Our results indicate that the DIFF-rGFP assay is a safe, efficient, and reliable platform for identifying viral protease inhibitors with potential applications in accelerating antiviral drug discovery.

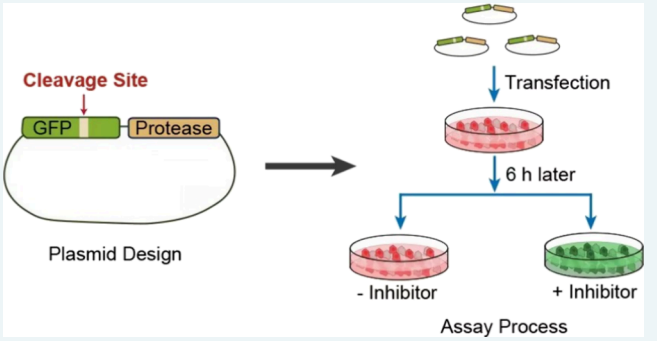

KEYWORDS: *antiviral drugs, recombinant GFP, protease, screening method*

Many viruses, including coronavirus, express their proteins as polyproteins containing one or more proteases. Such proteases autocatalytically release themselves from the precursor and cleave the remaining parts of the polyprotein into functional proteins.[1] Several viruses associated with significant human diseases, including retroviruses, flaviviruses, coronaviruses, and herpesviruses, code for a protease, which is indispensable for viral maturation and pathogenesis. Inhibition of this proteolytic activity can block the production of infectious viral progeny and reduce pathogenic processes;[1−4] these proteases inevitably become essential targets for antiviral drug development.[2]

SARS-CoV-2 $3CL^{pro}$ is a nonstructural protein that cleaves at least 11 sites on large viral polyproteins essential for replication and transcription.[5,6] Therefore, inhibiting the activity of $3CL^{pro}$ could disrupt SARS-CoV-2 viral replication, making it an attractive target for COVID-19 therapeutics. Furthermore, the structure of $3CL^{pro}$ is highly conserved across coronaviruses, indicating that it may be possible to develop pan-coronavirus inhibitors.[7]

Several methods have been used to screen protease inhibitors for antiviral drugs, mainly including noncell-based drug screening[8−14] such as FRET-based in vitro assay,[7] cell-based drug screening[15,16] such as cis cleavage luciferase assay,[17] live virus screening, or Flip-GFP assay.[18−20] Viral protease expression occurs intracellularly; therefore, small molecule protease inhibitors must enter cells to inhibit viral replication and proliferation. While in vitro assays using purified proteins can identify potential inhibitors, they fail to account for critical factors such as cell permeability and metabolic stability for small molecule inhibitors, which leads to inhibitors that are effective in vitro and ineffective in vivo. Meanwhile, live virus assays directly quantify viral replication (typically via plaque assays or quantitative RT-PCR) but face many challenges: difficulty in differentiating antiviral activity from cytotoxicity, higher biosafety requirements, and low suitability for high-

Received: April 11, 2025
Revised: September 3, 2025
Accepted: September 22, 2025
Published: October 9, 2025

https://doi.org/10.1021/acsptsci.5c00262
ACS Pharmacol. Transl. Sci. 2025, 8, 3944−3952

Table 1. Summary of the Insertion Sites

name	location	corresponding rGFP fluorescence maintain %[a]	name	location	corresponding rGFP fluorescence maintain %[a]
site1	W58−P59	0	site24	K159−N160	60.68 ± 0.40
site2	N145−Y146	0	site25	T10−G11	32.48 ± 1.06
site3	H149−N150	0	site26	Q70−C71	0
site4	D77−H78	0	site27	N160−G161	0
site5	F84−F85	0	site28	G175−S176	43.70 ± 2.31
site6	Y93−V94	0	site29	Q205−S206	0
site7	K102−D103	0	site30	V220−L221	0
site8	T119−L120	85.19 ± 0.73	site31	D118−T119	110.22 ± 0.86
site9	N106−Y107	0	site32	L120−V121	0
site10	E133−D134	0	site33	V121−N122	0
site11	E173−D174	46.49 ± 0.24	site34	A155−D156	53.57 ± 0.06
site12	K210−D211	0	site35	D156−K157	51.59 ± 1.05
site13	K215−R216	0	site36	K157−Q158	77.60 ± 0.58
site14	P197−D198	0	site37	N171−I172	26.60 ± 0.24
site15	Q158−K159	94.13 ± 0.95	site38	I172−E173	81.42 ± 0.81
site16	G25−H26	0	site39	D174−G175	34.43 ± 0.95
site17	Y40−G41	0	site40	S176−V177	35.21 ± 0.42
site18	P55−V56	0	site41	V177−Q178	0
site19	G139−H140	82.02 ± 0.78	site42	I153−M154	0
site20	G117−D118	69.78 ± 0.66	site43	M154−A155	23.54 ± 1.31
site21	P193−V194	0	site44	R169−H170	0
site22	F115−E116	0	site45	H170−N171	70.52 ± 0.00
site23	E116−G117	35.69 ± 1.18			

[a]Fluorescence intensity of 45 rGFP variants normalized to wild-type GFP. The values represent mean ± SD from triplicate experiments.

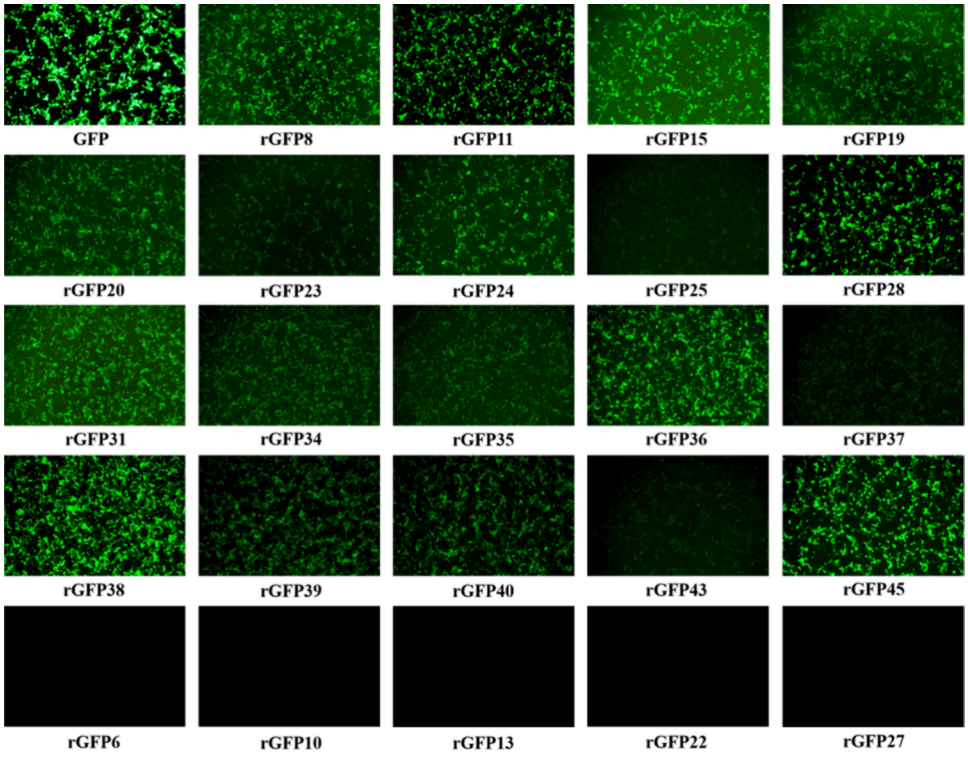

Figure 1. Representative images of recombinant GFPs. Fluorescence microscopy of recombinant GFP in HEK293T cells transfected with indicated plasmids for 48 h.

throughput screening. In addition, virtual screening and molecular dynamics simulations can identify candidate inhibitors; these computational approaches must be experimentally validated.[21]

Here, we present a novel fluorescence-based report assay (DIFF-rGFP) for identifying viral protease inhibitors in living cells. Unlike live virus screening, the DIFF-rGFP assay operates safely under BSL-1 containment, eliminating the need for higher-level biosafety facilities. Furthermore, the DIFF-rGFP system enables visual quantification of the inhibitor efficacy and is fully adaptable to high-throughput screening formats. Combining operational simplicity with robust scalability, the

https://doi.org/10.1021/acsptsci.5c00262
ACS Pharmacol. Transl. Sci. 2025, 8, 3944−3952

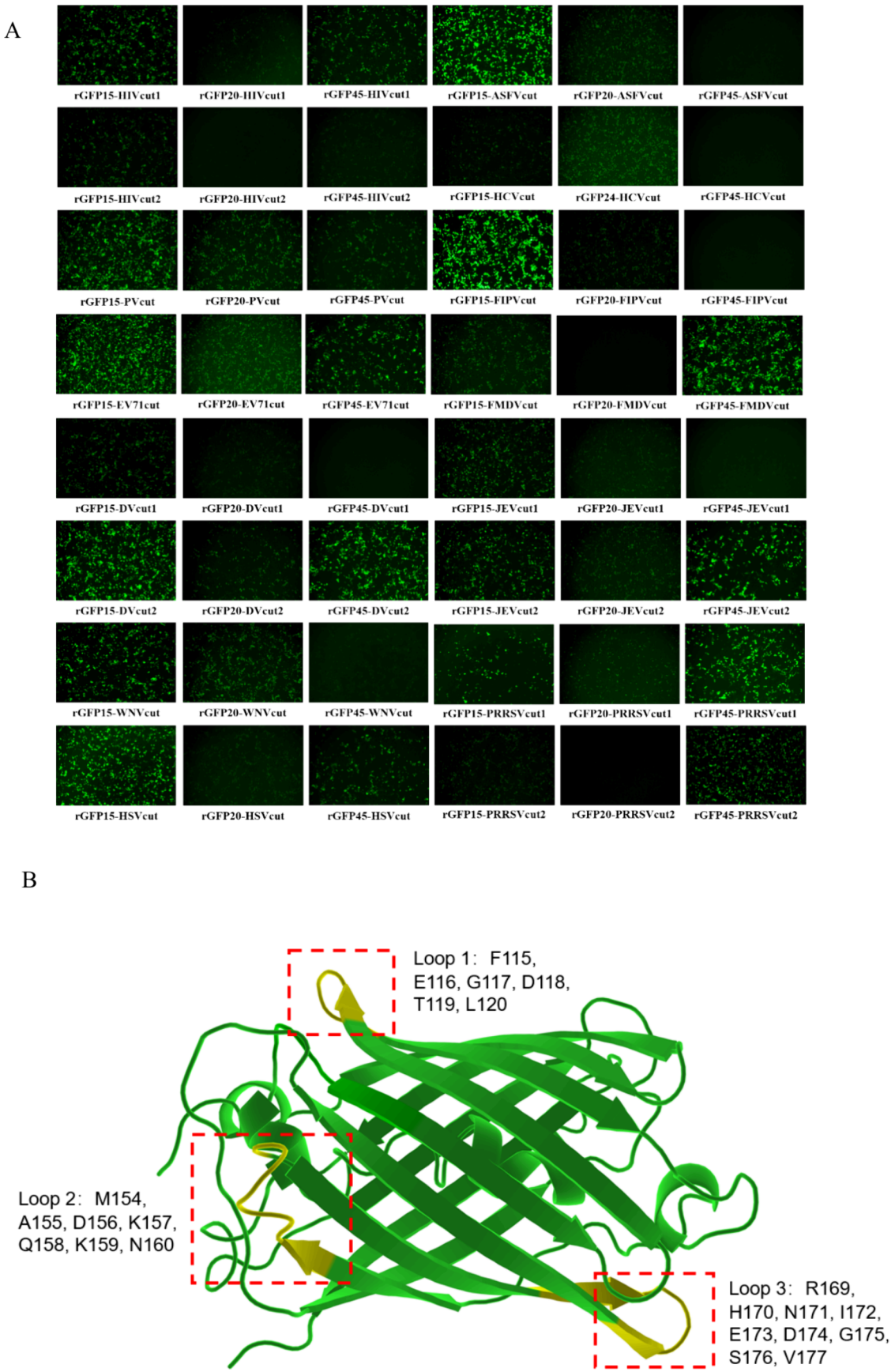

Figure 2. Flexible region test. (A) Insertion of various cleavage sequences into representative sites on three regions. There may exist more than one cleavage sequence for many viral proteases; we used two cleavage sequences named cut1 and cut2 for the protease from human immunodeficiency virus 1 (HIV), dengue virus (DV), West Nile virus (WNV), Japanese encephalitis virus (JEV), and porcine reproductive and respiratory syndrome

https://doi.org/10.1021/acsptsci.5c00262
ACS Pharmacol. Transl. Sci. 2025, 8, 3944−3952

Figure 2. continued

virus (PRRSV), respectively. For other viral proteases, we used one cleavage sequence, which was named cut. For example, rGFP15-HIVcut1 represents inserting HIVcut1 into site15 of GFP, rGFP15-PVcut represents inserting PVcut into site15 of GFP, and so on. (B) Corresponding locations of the available sites and flexible region within the GFP 3D structure (pdb: 1bfp),[23] yellow marked.

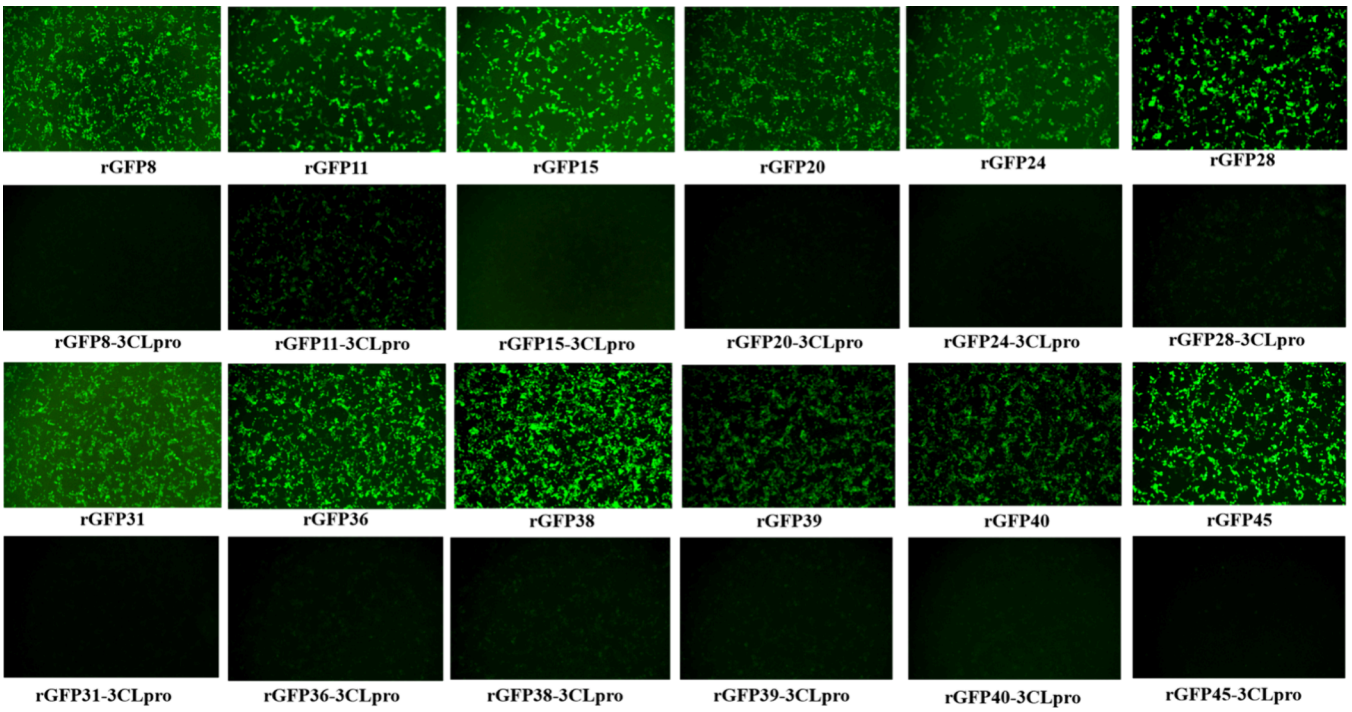

Figure 3. Coexpression of rGFP and protease in 293T cells. The pictures were captured 48 h after transfection.

DIFF-rGFP assay provides a powerful tool for accelerating antiviral drug discovery.

RESULTS

Screening GFP Insertion Sites for Viral Protease Cleavage Compatibility. Using the SARS-CoV-2 $3CL^{pro}$ cleavage motif (AVLQ↓SGFR),[22] we totally screened 45 GFP insertion sites for protease cleavage sequence compatibility. rGFP1−45 represents recombinant fluorescent proteins with insertion of SARS-CoV-2 $3CL^{pro}$ cleavage sequences into the corresponding site1−45 in Table 1. For instance, rGFP8 represents the insertion of the $3CL^{pro}$ cleavage sequence between T119 and L120 (site8) of GFP. It can be observed that among the selected 45 insertion sites, only 19 sites, i.e., sites 8, 11, 15, 19, 20, 23, 24, 25, 28, 31, 34, 35, 36, 37, 38, 39, 40, 43, 45, are compatible with the SARS-CoV-2 $3CL^{pro}$ protease cleavage sequence without significantly affecting the fluorescence of GFP or with only a limited impact. At the remaining sites, such as site6, site10, site13, site22, and site27, the fluorescence of GFP cannot be detected after inserting the $3CL^{pro}$ protease cleavage sequence (Figure 1). In the above 19 sites, site8, site15, site19, site31, and site38 maintained >80% fluorescence intensity compared to wtGFP; in addition, site20, site36, site24, and site45 maintained >60% fluorescence intensity compared to wtGFP. We adopted rGFPs with greater than 60% relative fluorescence intensity for the next studies.

By analyzing the above sites, three highly flexible regions that may accommodate exogenous short peptides are found. Region 1: E116 ∼ L120 (Table S1): The amino acid sequence of this region is EGDTL, and fluorescence is not detected in the region's near-neighboring site22, site32, and site33. Region 2: M154 ∼ N160 (Table S2): The amino acid sequence of this region is MADKQKN, and fluorescence is not detected in the region's near-neighboring site42, site43, and site27. Region 3: H170 ∼ V177 (Table S3): The amino acid sequence of this region is HNIEDGSV, and fluorescence is not detected in the region's near-neighboring site44 and site41.

GFP Compatible Regions Are Validated by Inserting Diverse Viral Protease Cleavage Sequences. To validate the generalizability of this method, we inserted multiple protease cleavage sequences from diverse RNA/DNA viruses into GFP compatible sites. The viral proteases and their corresponding cleavage sequences are listed in Table S4. First, we selected site15, site20, and site45, which are located in the three regions. Every viral cleavage sequence tested yielded functional GFP when inserted into at least one of the three flexible regions, except for the HCV cleavage sequence, which did not produce detectable fluorescence in the tested sites of site20 and site45. We then tried site24 and obtained the functional GFP (Figure 2A). The results demonstrated that for one single cleavage sequence, at least one site within the three regions would be available for insertion. Therefore, we propose that GFP contains three flexible regions capable of accommodating exogenous cleavage sequences.

Simultaneously, the sites and regions mentioned above were marked in the GFP 3D structure (Figure 2B). We could see that the three regions were mainly located in the loop domain or near the loop between the β strands of β4 and β5, β6 and β7, and β8 and β9. However, not all loops are feasible for insertion. Additionally, the Y92−G91 site was not located on

https://doi.org/10.1021/acsptsci.5c00262
ACS Pharmacol. Transl. Sci. 2025, 8, 3944−3952

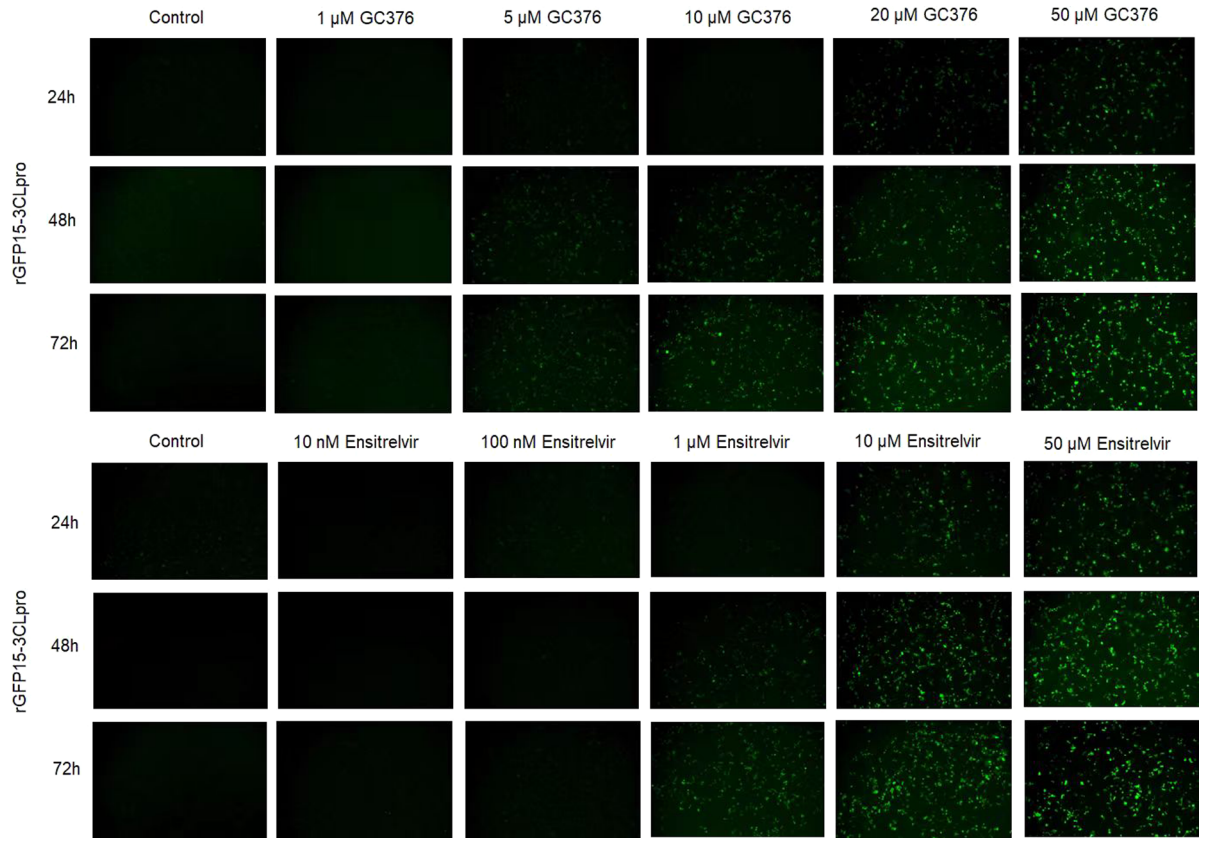

Figure 4. Validation of the rGFP assay of rGFP15-3CL^{pro}. Fluorescence intensity of rGFP15-3CL^{pro} in 293T cells treated with GC376 (0−50 μM) or ensitrelvir (0−50 μM) for 24, 48, and 72 h.

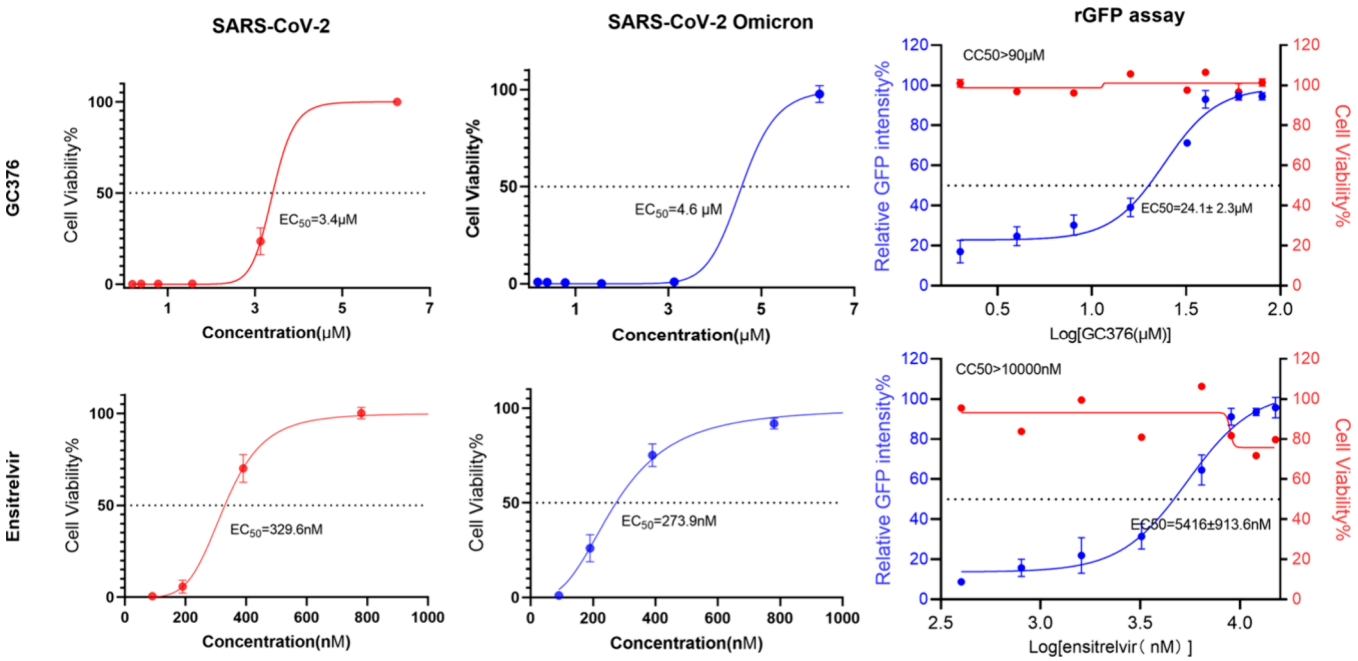

Figure 5. EC50 of the live virus and the rGFP15-3CL^{pro} assay.

the surface of the GFP, likely causing the lead cleavage sequence to be wrapped up and thus be protease-resistant.

Coexpression of the SARS-CoV-2 3CL Protease with rGFP Disrupts GFP Fluorescence. To confirm whether rGFP could be digested by the viral protease, we coexpression it with the SARS-CoV-2 3CL protease as a model. The sequence of 3CL^{pro} was added to the rGFP expression vector with a connection of P2A. Figure 3 shows that no green fluorescence was observed in rGFP variants (rGFP8, rGFP20, rGFP24, and rGFP31) when coexpressed with the 3CL^{pro} protease. Meanwhile, weak green fluorescence was still observed when rGFP11, rGFP15, rGFP28, rGFP36, rGFP38,

https://doi.org/10.1021/acsptsci.5c00262
ACS Pharmacol. Transl. Sci. 2025, 8, 3944−3952

rGFP39, rGFP40, and rGFP45 were coexpressed with the 3CL^{pro} protease. From then on, we confirmed that the viral protease could digest the cleavage sequence with relatively high efficiency, and it was realized that this system could be used for screening the protease inhibitors or evaluating the inhibitor. The fluorescence intensity investigated by ImageJ was provided in Table S5. When developing an EC50 assay for drug evaluation, both positive and negative controls need to be established. Based on data from Table S5, the positive control will be set as rGFP, and the negative control will be set as rGFP+Protease. Therefore, the smaller (rGFP+Protease)/rGFP is and/or the larger the rGFP-(rGFP+Protease) is, the higher the signal-to-noise ratio will be. The results indicated that pcDNA3.1-rGFP15-3CL^{pro} and pcDNA3.1-rGFP31-3CL^{pro} plasmids were preferable selections. Take the SARS-CoV-2 as an example, pcDNA3.1-rGFP15-3CL^{pro} plasmids were selected for further study comprehensively.

Assay Setup and Comparison. SARS-CoV-2 polyproteins are processed by two viral proteases, papain-like proteases (PL^{pro}) and 3CL^{pro}, which are excellent targets for the development of therapeutic antivirals. Some compounds have been validated targeting the 3CL^{pro}, such as GC376 and ensitrelvir, but some compounds still need to be investigated. Here, two compounds were chosen to develop the rGFP assay for 3CL^{pro} inhibitor screening. With the addition of GC376 up to 10 μM, green fluorescence reoccurred during the observation time. As the concentration increased, the fluorescence became brighter (Figure 4).

The same result was obtained for ensitrelvir except for a difference in the minimum active concentration, which is 1 μM.

Comparison of Different Assay Systems. The above results have demonstrated that the rGFP15-3CL^{pro} assay can be used to screen 3CL^{pro} protease inhibitor candidates. To understand the differences between the rGFP15-3CL^{pro} assay system and the live virus screening, we determined the EC50 of two small molecules, GC376 and ensitrelvir, based on the cell viability after SARS-CoV-2 infection and the GFP intensity, respectively. For GC376, the EC50 was 24.1 ± 2.3 μM of the rGFP15-3CL^{pro} assay, 3.4 μM of the live virus SARS-CoV-2 screening, and 4.6 μM of the live virus SARS-CoV-2 Omicron screening, respectively. For ensitrelvir, the EC50 was 5416 ± 913.6 nM of the rGFP15-3CL^{pro} assay, 329.6 nM of the live virus SARS-CoV-2 screening, and 273.9 nM of the live virus SARS-CoV-2 Omicron screening, respectively. The DIFF-rGFP assay differs by only an order of magnitude in sensitivity compared to the live virus (Figure 5). The differences between the DIFF-rGFP assay and live virus screening likely stem from the nature of the systems. In live virus assays, successful inhibition leads to a sharp reduction in viral replication, while failure results in exponential viral growth, producing a high signal. In contrast, the DIFF-rGFP assay exhibits a more gradual response, as it measures fluorescence intensity rather than viral replication directly. This smoother response may reduce the dynamic range of the assay but provides a more stable and reproducible readout. From then on, a cell-based, simple, and reliable DIFF-rGFP assay system was developed. Additionally, fluorescence can be measured by using a fluorescence spot counter, enabling high-throughput screening in 96-/384-well formats.

DISCUSSION

GFP is one of the most commonly used fluorescent proteins in scientific research, which is usually fused with the gene of interest at its N-terminal or C-terminal without influencing green fluorescence detection. The fluorescence expression is strictly related to the barrel-like structure, which is composed of the helical chromophore segment and eight β strands connected by 10 solvent-accessible loops; thus, little research inserted exogenous sequences into the internal of the GFP residuals. Although one research reported that the solvent-accessible loops are candidate sites for inserting random peptides, the sites or flexible region within GFP compatible with exogenous protease cleavage sequences still lack experimental evidence.[24] Only three sites have been validated upon the HCV NS3/4A cleavage sequence.[25]

In this work, we developed an easy-going detecting platform for protease inhibitor screening, which can be manipulated in a normal biosafety level lab. For the first time, we found the sites and flexible region competent in loading an exogenous viral protease cleavage sequence without affecting or with little affection on the green fluorescence intensity compared with wtGFP based on the SARS-CoV-2 3CL^{pro} cleavage sequence and other viral protease cleavage sequences. The most significant advantage is that for the unique exogenous sequence insertion, we can certainly seek out one or more proper sites within the flexible region of GFP, and the chromophore structure will not be prevented. When the exogenous sequences are inserted into the GFP, a recombinant green fluorescent reporting protein (rGFP) could be produced. Thus, researchers no longer need to take a lot of time studying from the beginning when designing rGFP or other fluorescently reported proteins homologous with GFP.

Second, we coexpressed the viral protease and the fluorescent report protein in one plasmid. Because the two genes were promoted by a shared promoter linked by a P2A self-cleaving sequence, the plasmids added into the cell medium tend to be more conveniently controlled compared with two separated plasmids, and the expression of the protease and rGFP is more stable in different cell types. Our following research indicated that the two genes could also be linked by a flexible linker and the protease cleavage sequence (data not shown). In this stage, the key point is that the protease cuts rGFP efficiently; otherwise, the fluorescence still exists. In some cases, we found that the protease could not digest the cleavage sequence so that the system did not work so well. Based on the above platform, a series of antiviral candidate screening assays can be developed targeting many positive single-stranded RNA viruses and some DNA viruses.[2]

Here, we also developed the rGFP reporter assays for SARS-CoV-2 3CL^{pro} and confirmed the inhibition activity of the small molecule GC376[26] and ensitrelvir.[27] The results showed that rGFP15-3CL^{pro} was a sensitive assay, which differs by only an order of magnitude in sensitivity compared to that of the live virus. Meanwhile in the assays, the EC50 was higher than the live virus screening. It was thought that the difference mainly came from the different characteristics between the virus and plasmid.

Comprehensively, the DIFF-rGFP assay inherently accounts for compound permeability and intracellular metabolic stability, which offer several key advantages for antiviral drug discovery. Compared with in vitro assays (e.g., FRET), it will exclude nonspecific cysteine protease inhibitors for which

https://doi.org/10.1021/acsptsci.5c00262
ACS Pharmacol. Transl. Sci. 2025, 8, 3944−3952

certain broad-spectrum cysteine protease inhibitors showed activity in cell-free systems but failed to inhibit the virus in cells, leading to yield false positives due to off-target inhibition of host proteases.[15,20,28] Moreover, by requiring simultaneous protease expression and inhibitor delivery within live cells, the DIFF-rGFP assay mimics physiological conditions that inherently filter out promiscuous binders. Thus, our system provides a more stringent and biologically relevant screening environment compared with traditional methods. However, compared to the gold standard FRET assay, our assay still suffers from low assay throughput and a long assay period.

MATERIALS AND METHODS

Plasmids, Cells, Viruses, and Drug Candidates. The pcDNA3.1(+) expression vector was preserved by our laboratory. 293T human embryonic kidney cells were obtained from the American Type Culture Collection (Manassas, Virginia, United States; catalog #CRL-3216) and maintained in Dulbecco's modified Eagle's medium supplemented with 2% fetal bovine serum (FBS). SARS-CoV-2 (wild-type and BA.5.2 strain) was provided by the Center for Disease Control and Prevention in Zhejiang Province, China. GC376 was obtained from Aladdin. Ensitrelvir and GC376 were obtained from MedChemExpress.

Plasmid Construction. Recombinant GFP (rGFP) was designed by inserting the protease cleavage sequence into the GFP coding sequence. The insertion sites were summarized in Table 1. PCR amplification was performed by Prime Star DNA polymerase (Takara). The GFP and rGFP were cloned into the multiple cloning site (MCS) of the pcDNA3.1(+) vector followed by the Uniclone One Step Seamless Cloning Kit instruction, respectively, producing the vector of pcDNA3.1-GFP and a series of pcDNA3.1-rGFPs. Subsequently, the viral protease was cloned at the 3′-terminal of the rGFP linked by a P2A peptide sequence, which produced plasmids coexpressing rGFP and SARS-CoV-2 $3CL^{pro}$ named pcDNA3.1-rGFP-$3CL^{pro}$. The protease cleavage sequences are summarized in Table S4.

Inhibitor Screening and rGFP Assay Development. We prepared 293T cells with a cell density of 5×10^5 cells/well for a 24-well plate. Plasmid transfections were carried out using lipofectamine 2000 according to the instructions. The drug candidates were dissolved in DMSO and diluted with DMEM. 4 h after transfection, the different concentrations of drug candidates were added into the corresponding wells and cultured for another 72 h. The green fluorescence was observed and pictured with a fluorescent microscope (OLYMPUS, CKX53). The fluorescence intensity was investigated by using ImageJ software.

Assay Validation. Before the experiment, the maximum nontoxic concentrations of small molecular compounds on Vero-E6 cells were investigated using Cell Counting Kit-8 (CCK-8) (Beyotime, Shanghai, China). The concentration with >80% cell survival rate was the maximum nontoxic concentration.

For the live virus experiment, Vero-E6 cells seeded in a 96-well plate were infected with 0.01 MOI of SARS-CoV-2 (wild-type or Omicron strain) at 37 °C for 1 h. After infection, the virus was discarded, and the cells were treated with 100 μL of different concentrations of drug candidates (6.25−0.39 μM for GC376 and 3.125−0.19 μM for ensitrelvir). For the virus control (VC) group, cells were covered with 100 μL/well of medium after infection. Cell control refers to cells without infection. After incubation at 37 °C for 3 days, the cells were rinsed twice with PBS and stained with MEM containing 10% CCK-8 for 1.5 h. The optical density values of each well were measured at 450 nm, and the cell viability was calculated.

For the rGFP assay, the 293T cells were seeded on a 96-well plate at 2.5×10^4 cells/well, and the coexpression plasmid was transfected following the lipofectamine 2000 transfection reagent kit instruction when the cell convergence reached 70−80%. The culture medium was replaced with fresh medium with different concentrations of drug candidates 4 h later, and the cells were cultured for 2 days at 37 °C and 5% CO_2. When detecting, the medium was discarded, and the fluorescence intensity was quantified by the multifunctional Enzyme Labeling Instrument (TECAN) at 485 nm excitation light and 535 nm absorption light. Positive control and negative blank control were set as the cells transfected with a 50 ng rGFP-expressing plasmid and cells transfected with an rGFP +Protease expressing plasmid, respectively. The relative GFP fluorescence intensity% .

$$= \frac{\mathrm{GFPintensity}_{drug} - \mathrm{GFPintensity}_{blank}}{\mathrm{GFPintensity}_{control+} - \mathrm{GFPintensity}_{blank}} \times 100\%$$

Quantification of GFP Fluorescence Intensity. Quantification of GFP fluorescence intensity was performed using Fiji/ImageJ. Images were converted to an 8-bit format and subjected to threshold-based segmentation. Mean gray values were measured exclusively within threshold-defined GFP-positive regions, background-corrected using cell-free areas, and normalized to untransfected controls.

Statistical Analysis. Statistical analysis was performed in GraphPad Prism 9.2.0 (GraphPad software, San Diego, California, United States). In Figure 5, the EC50 value was obtained by nonlinear regression that was performed for each data set with the best-fit value. For all experiments, at least three independent biological replicates were performed.

CONCLUSIONS

In summary, our study thoroughly investigated compatible sites or regions within the GFP and provided a lab-friendly, accurate, and efficient way for viral protease inhibitor screening, offering a framework to accelerate the time and effort in a cost-effective manner.

ASSOCIATED CONTENT

Supporting Information

The Supporting Information is available free of charge at https://pubs.acs.org/doi/10.1021/acsptsci.5c00262.

Details of GFP compatible regions and sites, the viral cleavage sequences, the fluorescence intensity of rGFP, and the coexpression of $3CL^{pro}$ catalytic mutants with rGFP (PDF)

AUTHOR INFORMATION

Corresponding Author

Beibei Wu − *Zhejiang Key Lab of Vaccine, Infectious Disease Prevention and Control, Department of Microbiology, Zhejiang Provincial Center for Disease Control and Prevention, Hangzhou 310015, China; School of Public Health, Hangzhou Medical College, Hangzhou 310053, China; School of Public Health, Wenzhou Medical University, Wenzhou 325035, China*; Email: bbwu@cdc.zj.cn

https://doi.org/10.1021/acsptsci.5c00262
ACS Pharmacol. Transl. Sci. 2025, 8, 3944−3952

Authors

Yan Feng − *Zhejiang Key Lab of Vaccine, Infectious Disease Prevention and Control, Department of Microbiology, Zhejiang Provincial Center for Disease Control and Prevention, Hangzhou 310015, China;* orcid.org/0000-0002-6885-725X

Xiaoyan Wu − *Zhejiang Difference Biological Technology Co., Ltd, Hangzhou 310000, China*

Ruiting Chen − *Zhejiang Difference Biological Technology Co., Ltd, Hangzhou 310000, China*

Yao Fan − *Zhejiang Difference Biological Technology Co., Ltd, Hangzhou 310000, China*

Changping Xu − *Zhejiang Key Lab of Vaccine, Infectious Disease Prevention and Control, Department of Microbiology, Zhejiang Provincial Center for Disease Control and Prevention, Hangzhou 310015, China*

Chenjie Fang − *Zhejiang Difference Biological Technology Co., Ltd, Hangzhou 310000, China*

Huimin Sun − *Zhejiang Difference Biological Technology Co., Ltd, Hangzhou 310000, China*

Shuling Jian − *Zhejiang Difference Biological Technology Co., Ltd, Hangzhou 310000, China*

Jiasheng Song − *Zhejiang Difference Biological Technology Co., Ltd, Hangzhou 310000, China*

Complete contact information is available at: https://pubs.acs.org/10.1021/acsptsci.5c00262

Author Contributions

†Y.F., X.W., and R.C. contributed equally to this work.

Author Contributions

‡J.S. and B.W. are co-senior authors.

Author Contributions

Conceptualization, Jiasheng Song; methodology, Xiaoyan Wu, Yan Feng, and Ruiting Chen; validation, Yan Feng and Changping Xu; formal analysis, Chenjie Fang and Huimin Sun; investigation, Shuling Jian; resources, Jiasheng Song and Beibei Wu; writing—original draft preparation, Yan Feng and Ruiting Chen; writing—review and editing, Yao Fan, Jiasheng Song, and Beibei Wu; supervision and project administration, Jiasheng Song; funding acquisition, Beibei Wu. All authors have read and agreed to the published version of the manuscript.

Notes

The authors declare no competing financial interest.

■ ACKNOWLEDGMENTS

This work was supported by the Basic Public Welfare Research Project of Zhejiang Province (LDT23H19013H19), the Key R&D Program of Zhejiang Province (2022C03188), and the Zhejiang Provincial Foundation for Scientific Research in Medicine and Health (WKJ-ZJ-2220).

■ ABBREVIATIONS

DIFF-rGFP,recombinant green fluorescent protein; rGFPs,recombinant green fluorescent proteins; $3CL^{pro}$,3-chymotrypsin-like protease; SARS-CoV-2,severe acute respiratory syndrome coronavirus-2; FRET,Förster resonance energy transfer; wtGFP,wild-type green fluorescent protein; HIV,human immunodeficiency virus; DV,dengue virus; WNV,West Nile virus; JEV,Japanese encephalitis virus; PRRSV,porcine reproductive and respiratory syndrome virus; HCV,hepatitis C virus

■ REFERENCES

(1) Tsu, B. V.; Fay, E. J.; Nguyen, K. T.; Corley, M. R.; Hosuru, B.; Dominguez, V. A.; Daugherty, M. D. Running With Scissors: Evolutionary Conflicts Between Viral Proteases and the Host Immune System. *Frontiers in immunology* **2021**, *12*, No. 769543.

(2) Majerová, T.; Konvalinka, J. Viral proteases as therapeutic targets. *Mol. Aspects Med.* **2022**, *88*, No. 101159.

(3) Schneider, J.; Kent, S. B. Enzymatic activity of a synthetic 99 residue protein corresponding to the putative HIV-1 protease. *Cell* **1988**, *54* (3), 363−8.

(4) Han, D. S.; Hahm, B.; Rho, H. M.; Jang, S. K. Identification of the protease domain in NS3 of hepatitis C virus. *J. Gen. Virol.* **1995**, *76* (Pt 4), 985−993.

(5) Durai, P.; Batool, M.; Shah, M.; Choi, S. Middle East respiratory syndrome coronavirus: transmission, virology and therapeutic targeting to aid in outbreak control. *Exp. Mol. Med.* **2015**, *47*, No. e181.

(6) Arya, R.; Kumari, S.; Pandey, B.; Mistry, H.; Bihani, S. C.; Das, A.; Prashar, V.; Gupta, G. D.; Panicker, L.; Kumar, M. Structural insights into SARS-CoV-2 proteins. *Journal of molecular biology* **2021**, *433* (2), No. 166725.

(7) Anand, K.; Ziebuhr, J.; Wadhwani, P.; Mesters, J. R.; Hilgenfeld, R. Coronavirus main proteinase (3CLpro) structure: basis for design of anti-SARS drugs. *Science* **2003**, *300* (5626), 1763−1767.

(8) Fu, L.; Ye, F.; Feng, Y.; Yu, F.; Wang, Q.; Wu, Y.; Zhao, C.; Sun, H.; Huang, B.; Niu, P.; Song, H.; Shi, Y.; Li, X.; Tan, W.; Qi, J.; Gao, G. F. Both Boceprevir and GC376 efficaciously inhibit SARS-CoV-2 by targeting its main protease. *Nat. Commun.* **2020**, *11*, 4417.

(9) Huff, S.; Kummetha, I. R.; Tiwari, S. K.; Huante, M. B.; Clark, A. E.; Wang, S.; Bray, W.; Smith, D.; Carlin, A. F.; Endsley, M.; Rana, T. M. Discovery and Mechanism of SARS-CoV-2 Main Protease Inhibitors. *Journal of medicinal chemistry* **2022**, *65* (4), 2866−2879.

(10) Ma, C.; Sacco, M. D.; Hurst, B.; Townsend, J. A.; Hu, Y.; Szeto, T.; Zhang, X.; Tarbet, B.; Marty, M. T.; Chen, Y.; Wang, J. Boceprevir, GC-376, and calpain inhibitors II, XII inhibit SARS-CoV-2 viral replication by targeting the viral main protease. *Cell research* **2020**, *30* (8), 678−692.

(11) Jin, Z.; Du, X.; Xu, Y.; Deng, Y.; Liu, M.; Zhao, Y.; Zhang, B.; Li, X.; Zhang, L.; Peng, C.; Duan, Y.; Yu, J.; Wang, L.; Yang, K.; Liu, F.; Jiang, R.; Yang, X.; You, T.; Liu, X.; Yang, X.; Bai, F.; Liu, H.; Liu, X.; Guddat, L. W.; Xu, W.; Xiao, G.; Qin, C.; Shi, Z.; Jiang, H.; Rao, Z.; Yang, H. Structure of Mpro from SARS-CoV-2 and discovery of its inhibitors. *Nature* **2020**, *582* (7811), 289−293.

(12) Rathnayake, A. D.; Zheng, J.; Kim, Y.; Perera, K. D.; Mackin, S.; Meyerholz, D. K.; Kashipathy, M. M.; Battaile, K. P.; Lovell, S.; Perlman, S.; Groutas, W. C.; Chang, K. O. 3C-like protease inhibitors block coronavirus replication in vitro and improve survival in MERS-CoV-infected mice. *Sci. Transl. Med.* **2020**, *12*, No. eabc5332.

(13) Wang, Y. C.; Yang, W. H.; Yang, C. S.; Hou, M. H.; Tsai, C. L.; Chou, Y. Z.; Hung, M. C.; Chen, Y. Structural basis of SARS-CoV-2 main protease inhibition by a broad-spectrum anti-coronaviral drug. *Am. J. Cancer Res.* **2020**, *10*, 2535−2545.

(14) Zhu, W.; Xu, M.; Chen, C. Z.; Guo, H.; Shen, M.; Hu, X.; Shinn, P.; Klumpp-Thomas, C.; Michael, S. G.; Zheng, W. Identification of SARS-CoV-2 3CL Protease Inhibitors by a Quantitative High-Throughput Screening. *ACS Pharmacol. Transl. Sci.* **2020**, *3*, 1008−1016.

(15) Ma, C.; Hu, Y.; Townsend, J. A.; Lagarias, P. I.; Marty, M. T.; Kolocouris, A.; Wang, J. Ebselen, Disulfiram, Carmofur, PX-12, Tideglusib, and Shikonin Are Nonspecific Promiscuous SARS-CoV-2 Main Protease Inhibitors. *ACS Pharmacol. Transl. Sci.* **2020**, *3*, 1265−1277.

(16) Cao, W.; Cho, C. D.; Geng, Z. Z.; Shaabani, N.; Ma, X. R.; Vatansever, E. C.; Alugubelli, Y. R.; Ma, Y.; Chaki, S. P.; Ellenburg, W. H.; Yang, K. S.; Qiao, Y.; Allen, R.; Neuman, B. W.; Ji, H.; Xu, S.; Liu, W. R. Evaluation of SARS-CoV-2 Main Protease Inhibitors Using a Novel Cell-Based Assay. *ACS central science* **2022**, *8* (2), 192−204.

(17) Rawson, J. M. O.; Duchon, A.; Nikolaitchik, O. A.; Pathak, V. K.; Hu, W. S. Development of a Cell-Based Luciferase Comple-

mentation Assay for Identification of SARS-CoV-2 3CLpro Inhibitors. *Viruses* **2021**, *13*, 173.
(18) Froggatt, H. M.; Heaton, B. E.; Heaton, N. S. Development of a Fluorescence-Based, High-Throughput SARS-CoV-2 3CLpro Reporter Assay. *Journal of virology* **2020**, *94* (22), e01265−20.
(19) Rothan, H. A.; Teoh, T. C. Cell-Based High-Throughput Screening Protocol for Discovering Antiviral Inhibitors Against SARS-COV-2 Main Protease (3CLpro). *Mol. Biotechnol.* **2021**, *63* (3), 240−248.
(20) Ma, C.; Tan, H.; Choza, J.; Wang, Y.; Wang, J. Validation and invalidation of SARS-CoV-2 main protease inhibitors using the Flip-GFP and Protease-Glo luciferase assays. *Acta pharmaceutica Sinica. B* **2022**, *12* (4), 1636−1651.
(21) Ibezim, A.; Onuku, R. S.; Ibezim, A.; Ntie-Kang, F.; Nwodo, N. J.; Adikwu, M. U. Structure-based virtual screening and molecular dynamics simulation studies to discover new SARS-CoV-2 main protease inhibitors. *Sci. Afr.* **2021**, *14*, No. e00970.
(22) Heilmann, E.; Costacurta, F.; Geley, S.; Mogadashi, S. A.; Volland, A.; Rupp, B.; Harris, R. S.; von Laer, D. A VSV-based assay quantifies coronavirus Mpro/3CLpro/Nsp5 main protease activity and chemical inhibition. *Commun. Biol.* **2022**, *5*, 391.
(23) Wachter, R. M.; King, B. A.; Heim, R.; Kallio, K.; Tsien, R. Y.; Boxer, S. G.; Remington, S. J. Crystal structure and photodynamic behavior of the blue emission variant Y66H/Y145F of green fluorescent protein. *Biochemistry* **1997**, *36* (32), 9759−65.
(24) Abedi, M. R.; Caponigro, G.; Kamb, A. Green fluorescent protein as a scaffold for intracellular presentation of peptides. *Nucleic acids research* **1998**, *26* (2), 623−30.
(25) (25.) Yan, X.; Shi, M. L.; Chen, N.; Wang, Y.; Zhang, Y.; Wang, Z.; Li, X. C.; Zhao, Z. H. Construction of a Fluorescence Detection Method for HCV NS3/4A Protease Activity. *China Biotechnol.* **2012**, *32*, 84−88.
(26) Heilmann, E.; Costacurta, F.; Moghadasi, S. A.; Ye, C.; Pavan, M.; Bassani, D.; Volland, A.; Ascher, C.; Weiss, A. K. H.; Bante, D.; Harris, R. S.; Moro, S.; Rupp, B.; Martinez-Sobrido, L.; von Laer, D. SARS-CoV-2 3CLpro mutations selected in a VSV-based system confer resistance to nirmatrelvir, ensitrelvir, and GC376. *Science translational medicine* **2023**, *15* (678), No. eabq7360.
(27) Syed, Y. Y. Ensitrelvir Fumaric Acid: First Approval. *Drugs* **2024**, *84* (6), 721−728.
(28) Ma, C.; Wang, J. Dipyridamole, chloroquine, montelukast sodium, candesartan, oxytetracycline, and atazanavir are not SARS-CoV-2 main protease inhibitors. *Proc. Natl. Acad. Sci. U. S. A.* **2021**, *118* (8), No. e2024420118.

https://doi.org/10.1021/acsptsci.5c00262
ACS Pharmacol. Transl. Sci. 2025, 8, 3944−3952